Phase Separation Dynamics and Pattern Formation in Thin Films of a Liquid Crystalline Copolyester in Its Biphasic Region

Wei Wang,[†,‡] Toshio Shiwaku,[†,§] and Takeji Hashimoto*[,†]

Department of Polymer Chemistry, Graduate School of Engineering, Kyoto University, Kyoto 606-8501, Japan, and State Key Laboratory of Functional Polymer Materials for Adsorption and Separation and Institute of Polymer Chemistry, College of Chemistry, Nankai University, Tianjin 300071, P. R. China

Received December 30, 2002

ABSTRACT: We present the experimental results concerning a phase separation dynamics and relevant pattern formation in thin film samples (ca. 10 μm in thickness) of a liquid crystalline copolyester in its biphasic region. The copolyester separates into an isotropic phase and an anisotropic phase in the biphasic region due to its composition heterogeneity, though it is homopolymer. The entire phase-separation process was in situ monitored in real space by polarized light microscopy. The structural evolution that appeared in the digital images was further analyzed using the fast Fourier transform method. The process can be described by the following steps: (1) The formation of a percolated network consisting of phase-separated isotropic and anisotropic liquids. The network growth obeys a scaling law $\Lambda_m(t) \propto q_m(t)^{-1} \propto t^{\alpha}$, where $\Lambda_m(t)$ is the characteristic length of the domains, $q_m(t)$ is the characteristic wavenumber, and t is the time. A crossover of the exponent from $^1/_3$ to $^1/_2$ was observed. (2) The network breaks up at a critical value of $\Lambda_m(t) = 50$ μm to form some anisotropic fragments with irregular shapes, followed by the further shrinking and reshaping into anisotropic drops. (3) The diffusion−coalescence of the drops to form large merged drops and the reshaping of these merged drops followed by orientational ordering within the merged drops. We studied the temperature dependence of these individual processes and discussed the mechanisms and the scaling behavior of the domain growth in the first step.

I. Introduction

In the past decades, there is much considerable attention on the dynamics of phase separation via spinodal decomposition in critical and off-critical binary polymer blends or other mixtures.[1,2] Almost all investigations show that the growth of domains in the late stage of phase separation in bulk or three dimensions (3D) obeys a scaling law given by $R(t) \propto t^{\alpha}$, where t is time, R is the average size of the domains, and α is an exponent, reflecting a universality of the phase separation process. Different values of the exponent describe different mechanisms controlling the domain growth: $\alpha = {}^1/_3$ and 1 for Lifshitz−Slyosov's growth without and with hydrodynamic interactions, respectively.[1−4]

We noted that in the past two decades the research attention was shifting to spinodal decomposition systems in thin films confined between two solid surfaces or between a solid surface and a free surface.[5−7] We collect the studies concerning the experimental observations of polymer mixtures in ref 5 and the works regarding the numerical simulations in ref 6. These previous studies show that the phase separation process in thin films becomes much more complex mainly because of the influences of the spatial confinement of the systems, the interactions with the surface or interface, the anisotropy of growths in various directions, and their couplings with each other. The confinement produces a loss in freedom, while the preferential attraction is able to cause a surface-directed spinodal decomposition in which the translational and rotational symmetry of phase-separated systems is broken and then the characteristic wave vectors are altered.[5a,d−g,j−l,6] The wave vectors parallel to the surface can grow faster than the perpendicular one. Moreover, both of them may grow in a way different from their bulk system. It has been confirmed by experimental observations and numerical simulations that the thin films may attain a bilayer or trilayer system caused by the preferential attraction of one of the components with the substrate surface or air after completion of phase separation. At the late stage the growth of the layer near the surface or interface obeys the scaling law $l(t) \propto t^{\alpha^{\perp}}$ for the domain growth normal to the surface (longitudinal domain growth designated by symbol $\perp$ in this study), where l is the layer thickness, in which $\alpha^{\perp} = {}^1/_3$ and 1 for systems without and with hydrodynamic interactions, respectively. At the same time, the previous studies[5b,c,h−k,6b,c] verify the scaling law as $R(t) \propto t^{\alpha^{\parallel}}$ for the lateral domain growth designated by the symbol ||. But the exponents are very conflicting as they range from $^1/_3$ to $^3/_2$, seemingly indicating a lack of the universality, an issue we would like to study in this work.

Currently, the effect of the orientational order parameter and its coupling with the concentration order parameter are also taken into account in studying the phase separation processes and mechanisms of the mixtures containing anisotropic liquid as one of components.[5i,8] In this study, we focus our attention on phase separation in the biphasic region of a main-chain thermotropic liquid crystal (LC) copolyester composed of rigid and flexible structure segments that statistically distribute along backbones. The rigid units provide the chain rigidity required for forming a LC phase, while the flexible units raise the flexibility of main chains in order to lower the temperature of forming a LC phase. When the molar fraction of the rigid units exceeds a

* To whom correspondence should be addressed.
† Kyoto University.
‡ Nankai University.
§ Present address: Polyplastics Co., Ltd., Research & Development Center, 973 Miyajima, Fuji 416, Japan.

10.1021/ma021790v CCC: $25.00
Published on Web 09/27/2003

certain value or when chain rigidity exceeds a critical value, the rigid macromolecules will self-assemble into an anisotropic LC phase.[9] For the chains with a given rigidity, as temperature is raised across a critical temperature, the rigidity will become lower than the critical value, so that a phase transition from the anisotropic phase to isotropic phase will occur. Moreover, the polydispersity in the molar mass and composition of the rigid and flexible units give rise to the polydispersity in chain rigidity. Because of this polydispersity, the phase transition occurs in a relatively broad temperature range, giving rise to a biphasic region composed of isotropic and anisotropic phases. In the biphasic region the LC copolymer phase-separates into the isotropic and anisotropic phases according to the polydispersity of the chain rigidity, and the two phases coexist at thermal equilibrium.

In this work, we experimentally studied the kinetics and pattern formation in the phase separation process of the thin film samples of the LC copolyester in its biphasic region. This phase separation was induced by rapidly increasing temperature of the specimens, which were initially in fully isotropic phase at a trapped nonequilibrium state as will be detailed in the following section, to various temperatures in the biphasic region. The phase separation process and the patterns formed were in-situ monitored by means of polarized light microscopy (PLM). The PLM generates images of high contrast between isotropic and anisotropic phases, which enable us to precisely explore the lateral growth of the domains. However, it does not allow us to easily follow the longitudinal domain growth. Hence, we only focus on the lateral phase separation in this work.

We observed the formation of a percolated network of the anisotropic phase in the isotropic matrix in the phase separation process. Our experimental observations and further analyses demonstrate a dynamic self-similarity on the lateral growth of the two-phase pattern that can be well described by the scaling law with the scaling exponent that crossovers from $^1/_3$ at the very early period in the late stage of phase separation process to $^1/_2$ at the late period in the late stage. When the domain grows to a critical size, the scaling law does not hold anymore. In this regime the breakup of the percolated anisotropic domains occurred due to instability of the domains caused by dewetting. The domain growth is much faster than that predicted by the scaling law. We studied the temperature effect and then discussed the mechanisms of the phase separation process of this system, in particular in the regime (regime I as will be defined later) in which the domain growth obeys the scaling law.

The present work is considered to be an extension of our earlier works[5i,10] on the phase separation and pattern formation processes for mixture of a thermotropic LC copolyester melt and an isotropic polyester melt to a homopolymer of LC copolyester with a considerable polydispersity in composition and hence in chain rigidity. The processes involved in these two systems will be elucidated to be quite similar, which highlights universal nature of the processes to be discussed in this work. Moreover, compared to the previous works,[5i,10] in this work a special focus will be shed on the processes in regime I, since the processes in other regimes are similar to those found and elaborated in the previous works. It should be pointed out that the present work is also relevant to the earlier work in ref 11.

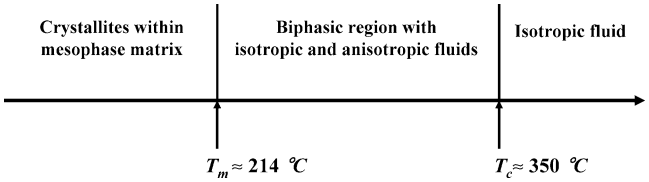

Figure 1. Various temperatures and states of the copolyester.

II. Experimental Section

The polymer used is a LC copolyester synthesized by a step polymerization of *p*-hydroxybenzoic acid (HBA) and ethylene terephthalate (ET). The synthesis and structure characterization will be briefly described in Appendix I. Here, we only state the specimen preparation, characterization, and analysis of the phase-separated structures and their evolution with time.

The copolyester was dissolved into *o*-chlorophenol at 80 °C to form a clear solution at a concentration of 2 wt %. The film specimens with a thickness of ca. 10 μm were prepared by casting two or three drops of the solution on bare microscopic cover glasses, which were cleaned by distilled water and then acetone, and then by quickly removing the solvent in a vacuum oven. The other side of the thin films thus prepared was left unconfined and exposed to air. All the details concerning specimen preparation had been given in our former works.[5i,10] The as-prepared "fresh" specimens were investigated under a polarized light microscope (PLM) (Nikon Optophot-Pol XTP-11), and we found that they are transparent, optically isotropic, and homogeneous under observation with the resolution that could be achieved by the normal optical microscopy. This indicates that we had successfully "frozen" a state of fully isotropic phase of the copolymer in the solid thin film specimens. The two-phase structure appearing in the thin film samples induced by rapidly increasing temperature to those in biphasic region (*T*-jump) were observed under the PLM equipped with a heating stage (Linkam Scientific Co. TH-600) preset at the selected temperatures. Under our experimental condition, the sample temperature can reach the temperature of the heating stage in a period shorter than ca. 3 s. We started to record the evolution of phase-separation process by a CCD camera in a frame of 460 pixels × 640 pixels at $t \geq 10$ s. As the domain grows with time, four lenses having different magnifications were used, so that the frame of 460 pixels × 640 pixels corresponds to areas having a size from ~195 μm × 270 μm to ~1510 μm × 2100 μm. The image data were simultaneously digitized with a software, and then a frame of 256 pixels × 256 pixels was selected for further analysis with an image analysis software (NIH image analysis 1.62).

III. Results

1. Formation of Phase-Separated Structure in Biphasic Region. The melting temperature of this copolyester is ~214 °C measured by a differential scanning calorimeter at a heating rate of 10 °C/min. Above 214 °C, we observed a change in the as-cast film from an optically isotropic film to an optically anisotropic viscous liquid. The behaviors and transition temperatures of this copolyester are shown in Figure 1. It is clear that this copolyester directly enters a relatively wide biphasic region from ~214 to 350 °C after melting.[12]

The typical evolution of the optical texture of a thin film sample after *T*-jump to 220 °C is demonstrated by the four PLM images in Figure 2. The image at $t = 0$ s was obtained for a sample before *T*-jump. The dark feature under PLM indicates that the as-prepared specimen is isotropic and homogeneous. The texture obtained at $t = 10$ and 20 s is optically anisotropic, but

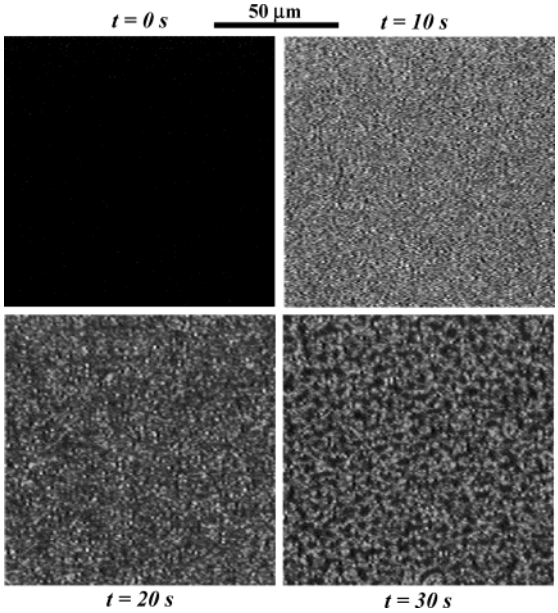

Figure 2. PLM images showing the formation of an anisotropic liquid and the subsequent phase separation into isotropic and anisotropic liquids in very early period at 220 °C.

its textural feature cannot be identified. However, we can see a coarsening of the texture when the time increases from 10 to 20 s. These are the typical features for most thermotropic LC copolyesters with high molecular weight. At t = 30 s we can see some small isotropic domains (the dark areas) phase-separated from the anisotropic matrix or network (the bright areas), that is, a feature to a two-phase texture in the initial period of the phase separation process. However, the contrast between the two phases is still low because of an overlay of the two-phase texture along the thickness direction. The formation of the two-phase structure in this system is driven by the thermodynamic instability of the system composed of molecules with the different chain rigidities. More rigid molecules tend to form a separated anisotropic phase in order to lower the free energy of the system.[9] Therefore, at the temperature above the melting point the copolyester liquid is subjected to a phase separation into an anisotropic phase containing the more rigid molecules and an isotropic phase containing the more flexible molecules.

2. Evolution of Phase-Separated Structure. After onset of the isothermal phase separation, the composition of the rigid and flexible molecules in each phase reaches an equilibrium one in the late stage of the phase separation where the two-phase structure will be coarsened in order to further lower the interfacial free energy of the system. The structural evolution in the biphasic region of this system at 220 °C is demonstrated by the PLM images shown in the left column of Figure 3. In Figure 3, we can see a very clear two-phase structure and its growth with increasing time from 100 to 900 s. The PLM images show a typical percolated network consisting of phases of anisotropic and isotropic liquids. The corresponding FFT patterns on the right column show circles with a single maxim that shifts to the lower region of scattering vector, q, with increasing time. At glance, these two-phase patterns are statistically similar to each other, indicating a structural growth with the dynamical self-similarity (we will confirm this issue later). This is the typical feature of a phase separation of a binary mixture system via spinodal decomposition

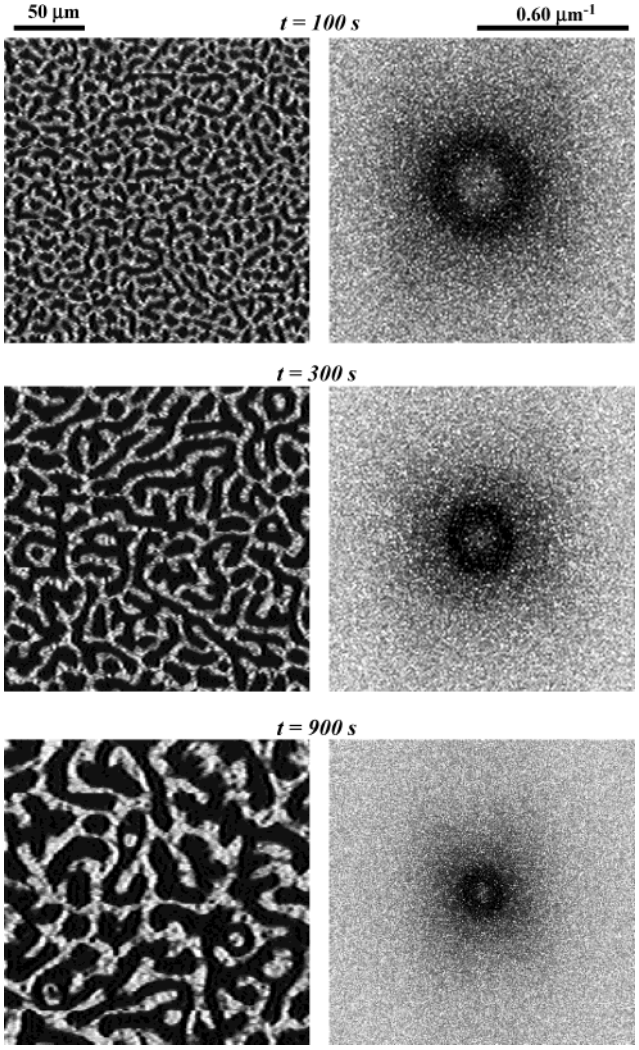

Figure 3. PLM images in the left column and the corresponding FFT patterns showing the growth of a percolated network formed by phase separation into isotropic and anisotropic liquids at 220 °C for 100, 300, and 900 s.

at the late stage. The dynamically self-similar growth keeps going on until about 2100 s at 220 °C. In this study, we designate this time domain and this characteristic phase-separation process as those in regime I. In the following section we will concentrate our attention on the growth mechanisms in this regime.

In Figure 4 the evolution of the two-phase structure at $t \geq 2100$ s is shown. Our observations show that the percolated network becomes very unstable, so it gradually disrupts or breaks into the many fragments. The image taken at t = 3900 s clearly illuminates the feature of a partially disrupted percolated network, while the image taken at t = 4800 s presents the textural feature after the percolated network was totally broken up. Here we can see many large anisotropic domains or fragments with irregular shape and many small anisotropic domains with circular shape. Sometimes, we can find some thin anisotropic fibrillar domains linking two large anisotropic domains. With further increasing time, the irregularly shaped anisotropic fragments shrink and then reshape into many anisotropic drops or droplets, as shown by the image taken at 5400 s. The drops having an average diameter of about 30−50 μm are formed by shrinkage and reshaping of large irregularly shaped domains, while the droplets having an average

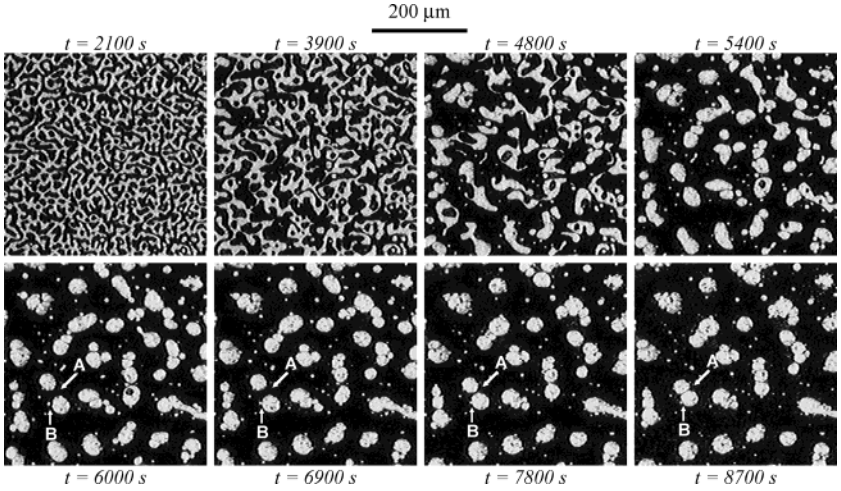

Figure 4. Top four PLM images showing a breaking up of the networks and the shrinking and reshaping of the broken anisotropic fragments with irregular shapes. Bottom images demonstrate the diffusion and coalescence of the anisotropic drops in the isotropic matrix.

diameter less than 10 μm are formed by the breakup of the thin fibrils. We note that the breakup of the percolated network is a process much slower than the process of the shrinking and reshaping of irregularly shaped anisotropic fragments. The former process completed in a time interval of about 2700 s as seen in the first image (t = 2100 s) to the third image (t = 4800 s) in Figure 4, while the latter one finished in a time interval of about 600 s as seen in the third image (t = 4800 s) to the fourth image (t = 5400 s) in Figure 4. In this work we designate this time domain (Δt = 2100−5400 s) as regime II.

In Figure 4, the four images in the bottom row show the structural evolution at $t \geq$ 6000 s, designated as regime III. The images with others (not shown here) demonstrate a coalescence and merging (or welding) process among the drops, a reshaping of the merged drops into a round shape, and an ordering inside the merged drops. The arrow A representatively points out a merging process of the two large drops, while the arrow B representatively shows a merging process of a large drop with a small droplet. We do not find out any similar events between two small droplets. These observations indicate that large drops move much faster than small droplets so as to decrease their interdomain distance. Although this result is the same as that found in the previous works,[5i,13] this is against a usual picture of diffusion of droplets in bulk driven by thermal activation processes.[1a,14] Most of the merged drops are noncircular in this time regime, indicating that the reshaping process is slow. We see clear boundaries in between two deformed drops after merging, indicating that the ordering process inside the merging drops is also very slow. These observations are different from those observed in bulk as well as the results found in thin polymer blends consisting of two flexible polymers.

3. Growth of Phase-Separated Domains and Scaling Behavior. The two plots in Figure 5 show the intensities $I(q)$ vs the scattering vector, q, determined from the FFT patterns of the optical images in Figures 3 and 4. Figure 5a shows the FFT power spectra in regime I where a single peak monotonically shifts to the low-q region with the increasing time, indicative of the simple growth of the two-phase structure. In Figure 5b, the four curves on $I(q)$ vs q obtained at 2100−5400 s (regime II) show a change in the shape of the spectra as well as that in the peak position, reflecting that the following two processes concurrently occurred in this regime as revealed from Figure 4 and also from a double-peak feature in the spectra: (1) the percolated networks breakup and (2) the shrinking and reshaping of the disrupted fragments. With a further increase of time from 6900 to 8700 s (regime III), the curves on $I(q)$ vs q show again only one peak at very low q region, and its position slowly shifts to the very lower q region, reflecting the growth of the domain structure due to coalescence of the drops as shown in Figure 4.

The values of characteristic length, $\Lambda_m \equiv 2\pi/q_m$, at different times were determined, and its time dependence at 220 °C is shown in the double-logarithmic plot in Figure 6. We can see a liner relation between log Λ_m and log t at 80 $\leq t \leq$ 2000 s (regime I), indicating existence of a scaling law between Λ_m and t as follows:

$$\Lambda_m(t) \propto q_m(t)^{-1} \propto t^{\alpha} \qquad (1)$$

The linear fitting of log $\Lambda_m(t)$ and log t plot shows $\alpha_I^{\parallel}$ = 0.460 with an error of ±0.004. This scaling behavior as well as our analysis showing the scaled structure factors of $I(q)/I(q_{max})$ vs q/q_{max} being independent of time (though not included in this paper), as reported in Figure 9 of our previous work,[5i] verifies the dynamical self-similar growth of the percolated anisotropic network in regime I. In this regime Λ_m increases from about 8 to 40 μm.

As shown in Figure 6, the linear relation between log $\Lambda_m(t)$ and log t starts to deviate after ∼2000 s. At first, we can see a slow increase of Λ_m from ∼30 to ∼65 μm when the time increases from about 2000 to 3500 s. This reflects the breakup of the percolated networks. When the time further increases from ∼3500 to 4000 s, Λ_m dramatically increases or jumps from ∼65 to ∼140 μm, reflecting a rapid shrinking and reshaping process. There is a linear relationship between log $\Lambda_m(t)$ and log t in this narrow time regime, and the linear fitting shows $\Lambda_m(t) \propto t^{\alpha_{II}^{\parallel}}$ with $\alpha_{II}^{\parallel}$ = 2.77 ± 0.043. It should be noted that the area fraction of the LC phase remarkably decreases in regime II down to a constant value attained in regime III. This is consistent with our previous observation,[5i] and the result is best interpreted as a consequence of protrusion of the LC domains along the direction normal to the thin film surface. The

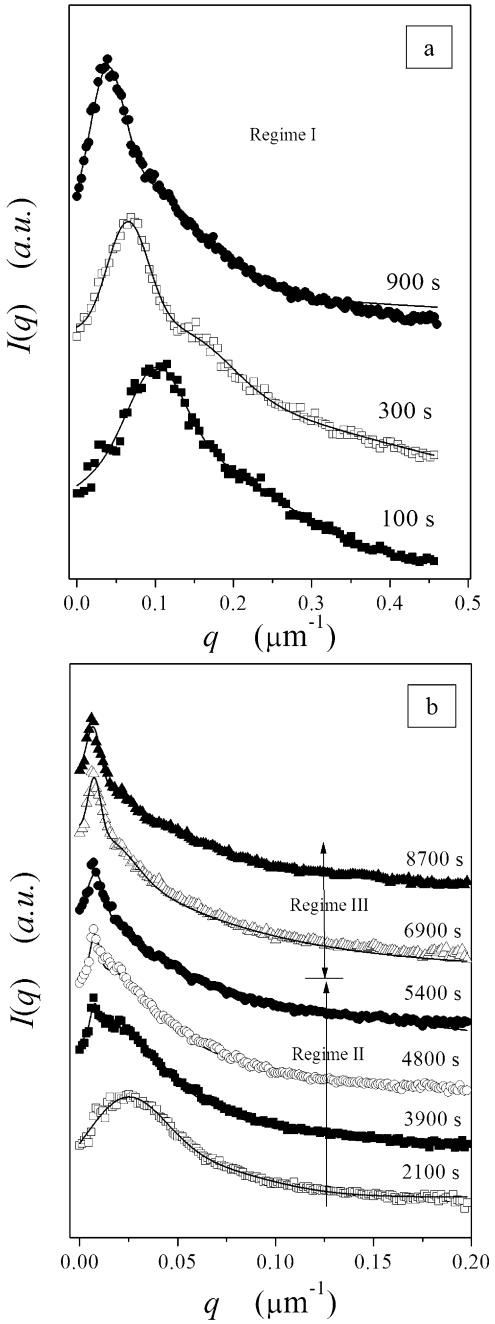

Figure 5. (a and b) Power spectra of the FFT patterns corresponding to the images shown in Figures 3 and 4. Clearly, the peak position monotonically shifts to the low-q region with increasing time.

protrusion is driven by dewetting of the LC domains from the glass substrate and naturally roughens the surface as clarified earlier.[5i] Thus, the roughening becomes increasingly obvious with time in regime II. This dewetting seems to become especially important, and concurrently the surface is expected to start roughening when the LC domains exceed a critical size of ~15 μm (corresponding to $\Lambda_m \cong 30$ μm) for this particular system. The protrusion of the LC domains triggered by dewetting naturally causes breakup of the LC domain networks, which accelerates the lateral growth rate of the domains as observed by the rapid increase of Λ_m with t, resulting in the large value of $\alpha_{II}^{||}$.

In regime III, the domain growth was caused by diffusion and coalescence of the anisotropic drops or droplets. Our observations indicate a scaling law $\Lambda_m(t) \propto t^{\alpha_{III}^{||}}$ with a small exponent $\alpha_{III}^{||} \approx 0.15$ or less. Because of very large drops (larger than a few tens of micrometers) and the size limitation of the sampling area, we realize that it is hard to accurately determine the exponent. So, we will not focus on $\alpha_{III}^{||}$ in this work.

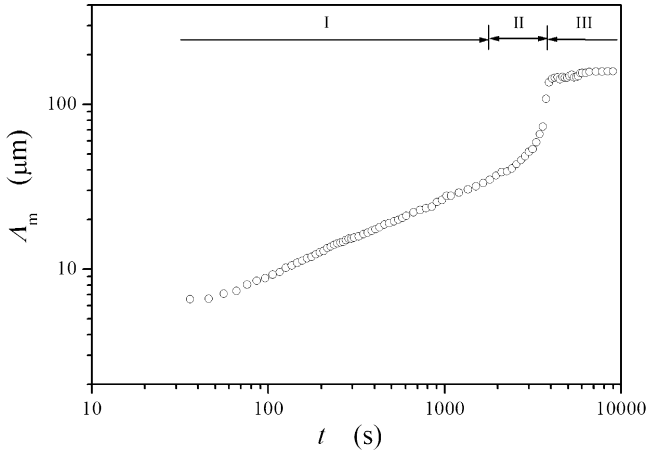

Figure 6. Double-logarithmic plot of Λ_m vs t at 220 °C.

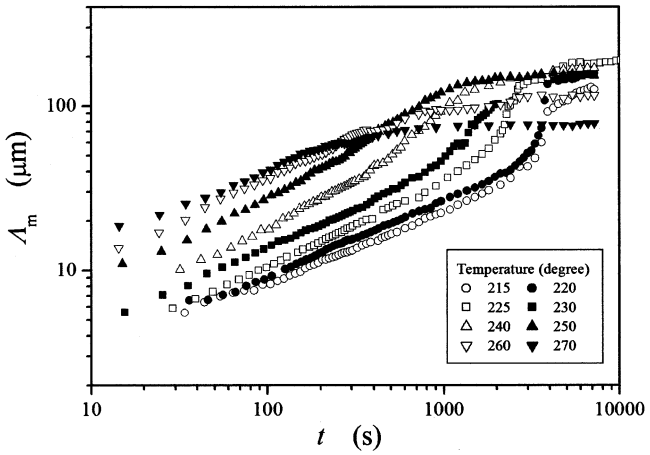

Figure 7. Double-logarithmic plots of Λ_m vs t at various temperatures as indicated in the figure.

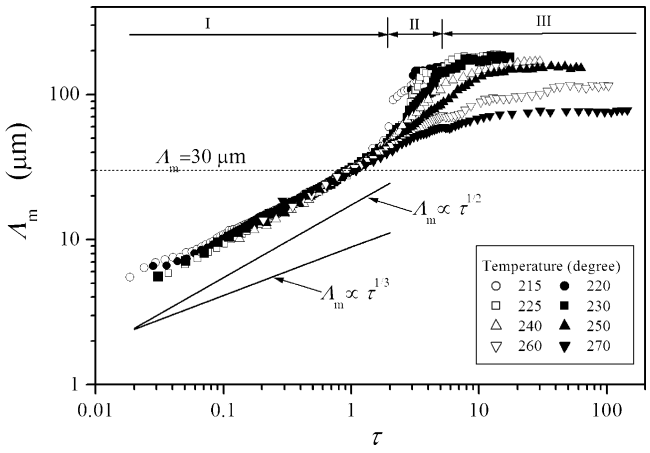

Figure 8. Double-logarithmic plots of Λ_m with reduced time τ.

4. Phase Separation Process at Different Temperature. Because of the wide biphasic region, we were able to carry out our experiments in the wide temperature range from 215 to 270 °C. The double-logarithmic plots of Λ_m vs t at the different temperatures in Figure

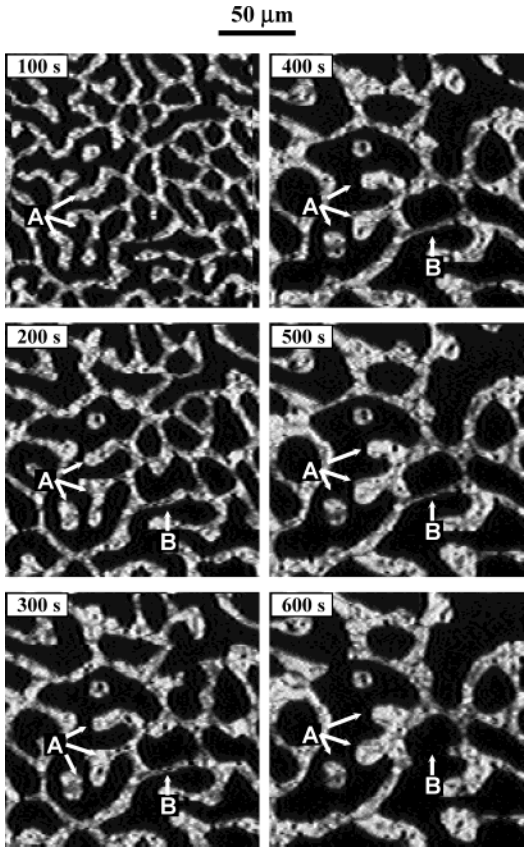

Figure 9. PLM images highlighting the mechanism of domain growth in regime I. Arrows A point out the some examples of shrinking and reshaping of the anisotropic arms, while arrow B shows a breaking-up process of a part of the anisotropic network.

Table 1. $\alpha_I^{||}$ and $\alpha_{II}^{||}$ Measured at the Eight Temperatures Covered in This Experiment

temp (°C)	$\alpha_I^{\|\|}$	$\alpha_{II}^{\|\|}$	temp (°C)	$\alpha_I^{\|\|}$	$\alpha_{II}^{\|\|}$
215	0.45	3.22	240	0.56	1.25
220	0.46	2.77	250	0.54	0.81
225	0.51	2.43	260	0.52	0.68
230	0.48	1.74	270	0.41	0.63

7 show the temperature effect on the phase separation process. At the eight temperatures selected, the growth of phase-separated domain structures can be also divided into three time regimes, as in the case at 220 °C. Most importantly, all eight curves in regime I show a linear relation between log $\Lambda_m(t)$ and log t. We can easily see the increase of the Λ_m values at a fixed time when the temperature raises from 215 to 270 °C. The values of $\alpha_I^{||}$ keep a constant value of ~0.5, as listed in Table 1: $\alpha_I^{||}$ changes in the range from 0.46 to 0.56 with an average of 0.493 ± 0.047. This indicates that the temperature change will not considerably alter the phase separation mechanisms in regime I. However, the crossover time from regime I to II decreases with increasing temperature. We found that $\alpha_{II}^{||}$ in regime II highly depends on temperature. In the temperature range from 215 to 270 °C, $\alpha_{II}^{||}$ gradually decreases from 3.3 to 0.63, as shown in Table 1. This evidently implies that the dewetting and hence the protrusion of the LC are temperature-dependent, seemingly decreasing with increasing temperature. This factor in turn may suppress the accelerated growth rate in regime II, giving rise to the decreasing $\alpha_{II}^{||}$ with temperature.

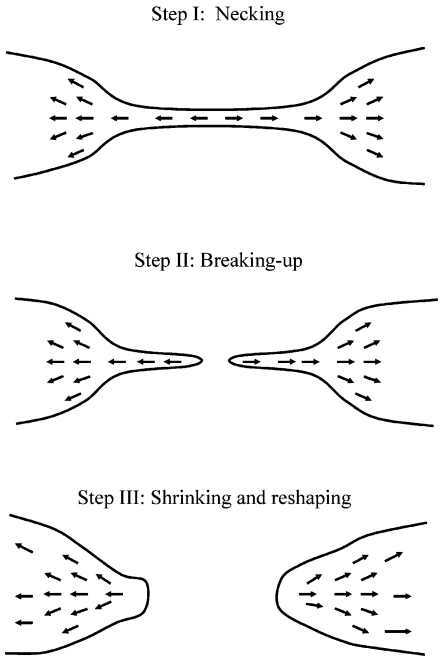

Figure 10. Schematic representation of possible steps of the entire processes of domain growth in regime I. Step I: formation of a neck zone in catenoidal channels. Step II: breakup of the thin LC domain. Step III: shrinking and reshaping of the broken domains.

5. Normalization of the Process in Regime I. In Figure 7 we can see the eight parallel straight lines in regime I; thus, we can get a master curve if we properly shift all curves on log $\Lambda_m(t)$ vs log t curves along log t axis. At first we define the time required to attain $\Lambda_m = 30\ \mu$m, denoted as t_{30} in the linear region between log $\Lambda_m(t)$ and log t, and then define a reduced time τ as follows:

$$\tau = \frac{t}{t_{30}} \tag{2}$$

Clearly, t_{30} is a function of temperature. Figure 8 shows a nearly perfect master curve for log $\Lambda_m(t)$ vs log τ. The solid lines in the figure show the scaling laws of $\Lambda_m \propto \tau^{1/2}$ and $\Lambda_m \propto \tau^{1/3}$. Clearly, at $\tau < 0.2$, $\alpha_I^{||}$ is slightly smaller than $^1/_2$ but seemingly close to $^1/_3$. At $0.2 < \tau < 2$, $\alpha_I^{||}$ is very close to $^1/_2$. At $\tau \approx 2$, $\Lambda_m \approx 50\ \mu$m, the system enters regime II in which the anisotropic network breaks up to form anisotropic fragments with irregular shape. Finally, this normalized plot can clearly demonstrate that the characteristic length Λ_m in regime III decreases with increasing temperature.

IV. Discussion

1. Domain Growth Mechanism in Regime I. Figure 9 highlights the mechanism of domain growth in regime I. All the images were taken from the same area of a thin film sample at 230 °C with a time interval of 100 s. The time domain covered ($100 \le t \le 600$ s) corresponds to $0.25 \le \tau \le 1.5$ (as $t_{30} \cong 400$ s) and hence to the later part of regime I. The arrows A point out the three examples of shrinking and reshaping of the anisotropic arms, while the arrow B shows a breakup process of a part of the anisotropic networks. To easily understand these processes, we schematically represent the possible steps of the entire processes of the domain growth in this system in Figure 10. In this figure, the

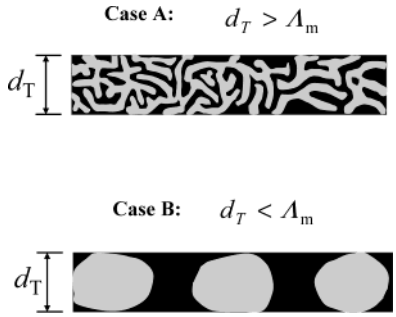

Figure 11. Schematic representations of the domain structure in the cross section of thin film samples of thickness d_T at different periods of phase separation. Case A corresponds to the early period at which $d_T > \Lambda_m$. Case B represents the later period with a feature of $d_T < \Lambda_m$.

arrows show the flow direction of anisotropic fluid. Our experimental observations elucidate the formation of a neck zone in the network as the first step for the breakup process of the network.[5i] This is due to the formation of catenoidal channels driven by thermal motion and thermodynamic instability (capillary wave fluctuation) of the network. LC molecules in the channel flow from the thinnest center toward the thickest ends of the channels and then orient along the flow direction. The driving force for the flow is the capillary pressure between the thinnest center and the thickest ends of the channels.[4,5i,11,15] Because of this flow, the channels become thinner and thinner; finally, it breaks up at a critical diameter of about 1 μm,[5i] resulting in an increase in network size and spacing. To further lower the interface free energy of the system, the broken-up arms will shrink and reshape into smoother network. The process and mechanism observed in this study are essentially identical to that found in our previous work.[5i]

2. Scaling Exponent in Regime I. The process and mechanism of the lateral domain growth are our major concern in this work. As briefly emphasized in the section I, almost all investigations confirmed the scaling law of the lateral domain growth as $R(t) \propto t^{\alpha||}$, but the exponents are still controversial. After a careful study of the results of the experimental observations[5] and numerical simulations,[6] we discuss two special cases in the late stage of phase separation process in the thin film samples, as schematically shown in Figure 11.

Case A represents a structure in a period in which the film thickness, d_T, is larger than the characteristic length, Λ_m, corresponding to an early period of the late stage of phase separation in thin film samples. The domain growth in longitudinal direction is essentially the same as that in the lateral direction. In other words, the phase separation process and mechanism are almost similar to those in bulk samples. The domain size will laterally grow following a scaling law as $\Lambda_m(t) \propto t^{\alpha||}$ in which $\alpha|| = {}^1/_3$ or 1 for systems without and with hydrodynamic interactions, respectively. Actually we can observe the $\tau^{1/3}$ behavior at $\tau < 0.2$ where $d_T > \Lambda_m$, as shown in Figure 8. This is an experimental verification of the numerical simulations obtained in thin film system by Marko[6a] and Puri et al.[6b] at the same period. It should be pointed out that the domain growth mechanism discussed in the previous subsection (IV.1) does not correspond to the domain growth in this period, but rather the later part in regime I where $d_T < \Lambda_m$ (case B).

In case B, $d_T < \Lambda_m$, representing a structure in a later period of regime I. The domain growth tends to be more restricted in the lateral direction as time elapses and become more close to two-dimensional (2D) phase separation of which the processes and mechanisms have been systemically studied through dimensional analyses[16] and numerical simulations.[17] These studies have demonstrated that the lateral domain growth should obey the scaling law as $\Lambda_m \propto t^{\alpha||}$ with $\alpha|| \leq {}^1/_2$. Clearly, the scaling behavior in 2D is different from that in 3D. The observed growth law, $\Lambda_m(t) \propto \tau^{1/2}$at $0.2 < \tau < 2$, confirms such scaling behavior. A similar scaling behavior ($\alpha|| = 0.44 \pm 0.02$) is also experimentally observed by Sung et al. in thin film samples of a polymer mixture with a 20 nm thickness.[5h] At the same time the numerical simulations of thin films carried out by Puri et al.[6b] and Toxvaerd[6c] reconfirmed this scaling behavior at the same period.

Obviously, there is a critical time where the crossover from case A to case B occurs. In our observation it occurs at $\tau \approx 0.2$, at which Λ_m reaches to d_T ($\approx$10 μm), independent of temperature, as demonstrated in Figure 8. Here we would like to mention an excellent work of the simulations on the phase separation of thin films, carried out by Puri et al.,[6b] in which they have demonstrated very similar phenomenon: the exponent crossover from $\sim{}^1/_3$ to $\sim{}^1/_2$ at a critical time. They further show that the critical time increases with the thickness, meaning that the crossover occurs later in the thicker sample, giving rise to a further support to our observation regarding the crossover of the phase separation mechanism at $d_T \approx \Lambda_m$. As Puri et al. pointed out,[6b] the faster growth with $\sim{}^1/_2$ exponent is probably due to a part of network (between neighboring branch points and/or between a branch point and a free end of the branch) being broken up to result in elongated strands parallel to the substrate surface even in regime I. This had been observed by our experimental observation, as demonstrated by the PLM images in Figure 3 (see the images at $t = 300$ and 900 s in the regime of $\Lambda_m > d_T$).

Finally, we note that the scaling behaviors are different from those presented in our previous works in which we found a ${}^1/_3$ exponent in a mixture of isotropic PET melt with a LC copolyester melt at 260, 270, and 280 °C, the biphasic region of the LC copolyester.[5i] This difference reflects the complexity of the phase separation in thin films, which can be interpreted by a current 2D simulation. Novik and Coveney stated that scaling exponents will gradually decrease from ca. ${}^1/_2$ at critical composition to ca. ${}^1/_3$ at highly off-critical composition.[18] Assuming it is the case, the blend system studied in the previous work is much far from critical composition in comparison with present work at the same temperature (270 °C), so that exponents observed in this work may be larger than ${}^1/_3$ obtained in the previous work. However, this scenario is not thoroughly confirmed yet, as the phase diagrams of the two experimental systems have been unveiled yet.

3. Kinetics of Phase Separation in Regime I. Figure 12 shows the Arrhenius plots of ln t_{30} and ln t_{50} with $1/T$ where t_{50} is the time when Λ_m becomes equal to 50 μm. The linear fitting shows an activation energy of $\Delta E = 160 \pm 10$ kJ/mol for t_{30}, very consistent with the activation energy ($\sim$160 kJ/mol) measured from a similar LC polyester in its LC region (225−250 °C) using a capillary rheometry.[19] This consistency again indicates that the flow and orientation of the LC phase in the catenoidal channels of the isotropic phase governs the growth of the percolated network pattern, as schemati-

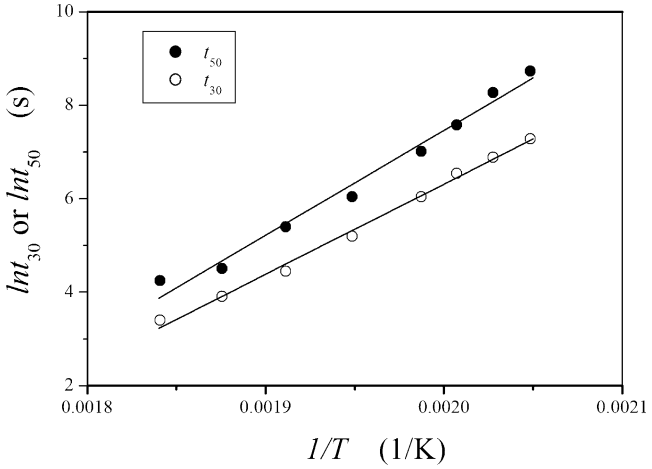

Figure 12. Arrhenius plots of ln t_{30} and ln t_{50} with $1/T$. The activation energies were determined by linear fitting of the experimental data.

cally shown in Figure 10. Therefore, Λ_m as the function of t and T in the major part of regime I can be ascribed as follows:

$$\Lambda_m(t,T) = Ae^{\Delta E/RT}t^{\alpha_I^{||}} \quad (3)$$

in which $A = 9.86 \times 10^{-15}$, $\Delta E = 160 \pm 10$ kJ/mol, and $\alpha_I^{||} \approx 0.5$. The activation energy for t_{50} is $\Delta E = 185 \pm 15$ kJ/mol, slightly larger than $\Delta E = 160 \pm 10$ kJ/mol obtained from ln t_{30} vs $1/T$ since t_{50} describes the critical time when the percolated network starts to break up. Some other processes may come into play in the coarsening of the anisotropic networks that makes ΔE larger.

V. Conclusion

We have studied the phase-separation dynamics and the relevant pattern formation of the LC copolyester in its biphasic region. The samples were prepared by casting solution of the copolyester into ~10 μm thick films. The thin films were optically isotropic and homogeneous and hence used as those vitrified from fully isotropic melts of the copolyester. Because of the formation of an isotropic phase and an anisotropic phase after the phase separation in the biphasic range, we in situ monitored the entire phase-separation processes in real space with PLM and then analyzed the structural evolution using the FFT method.

The entire processes in the biphasic region can be described by the following steps: Regime I: the formation of a percolated network consisted of phase-separated isotropic and anisotropic liquids. Regime II: the network breaks up at a critical value to form some anisotropic fragments with irregular shape, followed by the further shrinkage and reshaping into many anisotropic drops or droplets. Regime III: the coalescence of the drops or droplets by diffusion to form large merged drops and the ordering and reshaping of these merged drops. We found that in regime I the percolated network growth obeys the scaling law $\Lambda_m(t) \propto q_m(t)^{-1} \propto t^{\alpha_I^{||}}$ before the network breaks up at $\Lambda_m(t) = 50$ μm. At $\Lambda_m < 15$ μm $\alpha_I^{||}$ is seemingly close to $^1/_3$ because of the 3D structure feature. At $15 < \Lambda_m < 50$ $\alpha_I^{||}$ is very close to $^1/_2$, a typical scaling exponent of domain growth in the late stage of spinodal decomposition in thin films or 2D. The temperature dependence of the domain growth revealed that $\alpha_I^{||}$ is independent of temperature, and hence the mechanism of the percolated network growth keeps unchanged with temperature. The activation energy measured in this work is $\Delta E = 160 \pm 10$ kJ/mol, very consistent with the activation energy (~160 kJ/mol) measured from a similar LC copolyester in its LC region by rheometry. This consistency indicates that the flow and orientation of the LC molecules in the catenoidal channels govern the growth of the percolated network pattern.

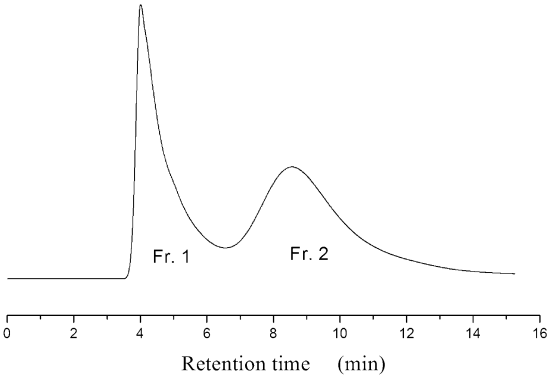

Figure 13. HPLC graph of the LC copolyester used in this work, showing a dual-composition distribution feature. The area ratio of the two fractions is close to unity.

In this work the phase separation dynamics was studied for unconfined thin films of the copolyester prepared on the bare glasses. It may be interesting and important to compare the results with those obtained for surface-treated glasses or for the films sandwiched between two glasses to clarify effects of preferential attractions of one of the components with surfaces on the phase separation dynamics.

Appendix I. Characteristics of LC Copolyester

The copolyester was synthesized by a step polymerization of *p*-hydroxybenzoic acid (HBA) and ethylene terephthalate (ET) following the conditions reported in ref 20. The molar ratio of two monomers used is unity. This selection is based on the reported results that the copolyester with the same ratio shows a broad biphasic region from its melting temperature (~214 °C) to its clearing temperature (>350 °C) which gives us a chance to study the kinetics of phase separation in such a wide temperature region.[12]

To seek out the possible origin of the wide temperature range for biphasic structure, an analysis of the composition distribution of HBA and ET units in this copolyester was carried out by using high-performance liquid chromatography (HPLC) with chlorophenol as a solvent. A dual-composition distribution feature was characterized, as shown in Figure 13. Further NMR analysis indicates that the fraction I (Fr. 1 in the figure) contains 58% HBA units while the fraction II (Fr. 2) contains 47% HBA units, implying that on average the copolyester molecules in fraction I have a chain rigidity higher than the molecules in fraction II. This difference will cause a difference in ability of LC formation between the two fractions. Definitely, in comparison with the molecules in fraction II, the molecules in fraction I should show a stronger ability in forming a LC phase at the same conditions. This special polydispersity is totally different from the polydispersity caused by a random distribution of the two segments or/and a molecular weight distribution. The dual-composition

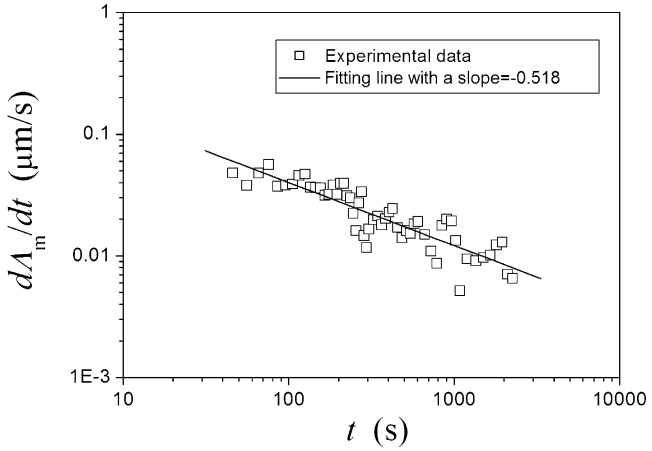

Figure 14. Plot of log [d$\Lambda_m(t)$/dt] vs log t. The data used for the analyses are those presented in regime I of Figure 6. Fitting the data gives the slope of −0.52.

distribution originally comes from the difference in the reactivity of two kinds of monomers.[20] In a sense this copolyester can be treated as a polymeric mixture composed of two components corresponding to Fr. 1 and Fr. 2. Anyway, it is worth mentioning that the area ratio of the two fractions is close to unity, similar to the molar ratio of two monomers.

Appendix II. Scaling Law, $\Lambda_m(t) \propto t^\alpha$, in Regime I

As presented above, a two-phase structure having a size of micrometer level has been observed at an initial stage of our observation. The image taken at $t = 30$ s in Figure 2 is a typical example. In general, the time evolution of $\Lambda_m(t)$ may be written as

$$\Lambda_m(t) = \Lambda^{SD} + \text{constant} \times t^\alpha \qquad (4)$$

where Λ^{SD} denotes the characteristic length developed at the early stage of spinodal decomposition and hence is independent of time. Clearly, this coarsening law is different from the scaling law, $\Lambda_m(t) \propto t^\alpha$ (eq 1), used earlier. If eq 4 is valid, the slope of $\log(\Lambda_m(t) - \Lambda^{SD})$ vs log t plot gives the correct exponent α. If $\Lambda_m(t) \gg \Lambda^{SD}$; however, there would be little difference between eq 1 and eq 4. However, if $\Lambda_m(t)$ is close to Λ^{SD}, the exponents α obtained by eqs 1 and 4 should be very different because the constant value affects significantly the value α. One way to analyze the value α based on eq 4 is to plot $\log(d\Lambda_m(t)/dt)$ vs $\log(t)$,

$$d\Lambda_m(t)/dt = \alpha \times \text{constant} \times t^{\alpha-1} \qquad (5)$$

A typical example of such a plot is shown in Figure 14. The data used for this analysis are those presented in regime I of Figure 6 obtained at 220 °C. Fitting the data of $\log(d\Lambda_m(t)/dt)$ vs log t gets a slope ≈−0.52 with a correlation coefficient of $R = -0.885$. This means $\alpha \approx 0.48$, which is close to 0.46 obtained according to the scaling law of eq 1, meaning that the time covered in our experiment is long enough so that the value Λ^{SD} is relatively small compared with the second term of right-hand side of eq 4. In conclusion, the scaling law $\Lambda_m(t) \propto t^\alpha$ used in this work is reasonable.

References and Notes

(1) (a) Gunton, J. D.; Miguel, M. S.; Sahni, P. S. In *Phase Transition and Critical Phenomena*; Domb, C., Lebowitz, J. L., Eds.; Academic: New York, 1983; Vol. 8. (b) Furukawa, H. *Adv. Phys.* **1983**, *34*, 703. (c) Bray, A. J. *Adv. Phys.* **1994**, *43*, 357.
(2) (a) Hashimoto, T. *Phase Transitions* **1988**, *12*, 47. (b) In *Dynamics and Patterns in Complex Fluids*; Onuki, A., Kawasaki, K., Eds.; Springer: Berlin, 1990. (c) Hashimoto, T. In *Materials Science and Technology*; Cahn, R. W., Haasen, P., Kramer, E. J., Eds.; Structure and Properties of Polymers Vol. 12, Thomas, E. L., Vol. Ed.; VCH: Weinheim, 1993; Chapter 6.
(3) Lifshitz, I. M.; Slyozov, V. V. *Phys. Chem. Solids* **1961**, *19*, 35.
(4) Siggia, E. D. *Phys. Rev. A* **1979**, *20*, 595.
(5) (a) Jones, R. A. L.; Norton, L. J.; Kramer, E. J.; Bates, F. S.; Wiltzius, P. *Phys. Rev. Lett.* **1991**, *66*, 1326. (b) Wiltzius, P.; Cumming, A. *Phys. Rev. Lett.* **1991**, *66*, 3000. (c) Wiltzius, P.; Cumming, A. Bates, F. S.; Rosedale, J. H. *Phys. Rev. A* **1992**, *45*, 885. (d) Bruder, F.; Brenn, R. *Phys. Rev. Lett.* **1992**, *69*, 624. (e) Kruasch, G.; Dai, C.-A.; Kramer, E. J.; Bates, F. S. *Phys. Rev. Lett.* **1993**, *71*, 3669. (f) Kruasch, G.; Dai, C.-A.; Kramer, E. J.; Marko, J. F.; Bates, F. S. *Macromolecules* **1993**, *26*, 5566. (g) Straub, W.; Bruder, F.; Brenn, R.; Krausch, G.; Bielefeldt, H.; Kirsch, A.; Marti, O.; Mlynek, J.; Marko, J. F. *Europhys. Lett.* **1995**, *29*, 353. (h) Sung, L.; Karim, A.; Douglas, J. F.; Han, C. C. *Phys. Rev. Lett.* **1996**, *76*, 4368. (i) Nakai, A.; Shiwaku, T.; Wang, W.; Hasegawa, H.; Hashimoto, T. *Macromolecules* **1996**, *29*, 5990. Nakai, A.; Wang, W.; Ogasawara, S.; Hasegawa, H.; Hashimoto, T. *Macromolecules* **1998**, *31*, 5391. (j) Heier, J.; Kramer, E. J.; Revesz, P.; Battistig, C.; Bates, F. S. *Macromolecules* **1999**, *32*, 3758. (k) Wang, H.; Composto, R. J. *Phys. Rev. E* **2000**, *61*, 1659; *J. Chem. Phys.* **2000**, *113*, 10386. (l) Geoghegan, M.; Ermer, H.; Jüngst, G.; Krausch, G.; Brenn, R. *Phys. Rev. E* **2000**, *61*, 940.
(6) (a) Marko, J. F. *Phys. Rev. E* **1993**, *48*, 2863. (b) Puri, S.; Binder, K.; Frisch, H. L. *Phys. Rev. E* **1997**, *56*, 6991. (c) Toxvaerd, X. *Phys. Rev. Lett.* **1999**, *83*, 5318.
(7) For reviews of experimental studies of this problem, see: Kruasch, G. *Mater. Sci. Eng. Rep.* **1995**, *14*, 1. For reviews of numerical simulations of this problem, see: Binder, K. *J. Non-Equilib. Thermodyn.* **1998**, *23*, 1; *Adv. Polym. Sci.* **1999**, *138*, 1.
(8) (a) Fukuda, J. *Phys. Rev. E* **1998**, *58*, 6939; **1999**, *59*, 3275. (b) Matsuyama, A.; Evans, R. M. L.; Cates, M. E. *Phys. Rev. E* **2000**, *61*, 2977.
(9) Flory, P. J. *Proc. R. Soc. London, Ser. A* **1956**, *234*, 73; *Adv. Polym. Sci.* **1984**, *59*, 1.
(10) Nakai, A.; Shiwaku, T.; Wang, W.; Hasegawa, H.; Hashimoto, T. *Polymer* **1996**, *37*, 2259.
(11) (a) Nakai, A.; Wang, W.; Hashimoto, T.; Blumstein, A.; Maeda, Y. *Macromolecules* **1994**, *27*, 6963. (b) Nakai, A.; Wang, W.; Hashimoto, T.; Blumstein, A. *Macromolecules* **1996**, *29*, 5288.
(12) (a) Lenz, R. W.; Jin, J. I.; Feichtinger, K. A. *Polymer* **1983**, *24*, 327. (b) Nicely, V. A.; Dougherty, J. T.; Renfro, L. W. *Macromolecules* **1987**, *20*, 573.
(13) Nagaya, T.; Orihara, H.; Ishibashi, Y. *J. Phys. Soc. Jpn.* **1989**, *58*, 3600.
(14) (a) Binder, K.; Stauffer, D. *Phys. Rev. Lett.* **1974**, *33*, 1006. (b) Binder, K. *Phys. Rev. B* **1977**, *15*, 4425.
(15) Rey, A. D. *Macromolecules* **1997**, *30*, 7582.
(16) (a) San Miguel, M.; Grant, M.; Gunton, J. D. *Phys. Rev. A* **1985**, *31*, 1001. (b) Grant, M.; Elder, K. R. *Phys. Rev. Lett.* **1999**, *82*, 14.
(17) (a) Koch, S. W.; Desai, R. C.; Abraham, F. F. *Phys. Rev. A* **1983**, *27*, 2152. (b) Valls, O. T.; Mazenko, G. F. *Phys. Rev. B* **1988**, *38*, 11643. (c) Velasco, E.; Toxvaerd, S. *Phys. Rev. Lett.* **1993**, *71*, 388. (d) Ossadnikm, P.; Gyure, M. F.; Stanley, H. E.; Glotzer, S. C. *Phys. Rev. Lett.* **1994**, *72*, 2498.
(18) Novik, K. E.; Coveney, P. V. *Phys. Rev. E* **2000**, *61*, 435.
(19) Cuculo, J. A.; Chen, G.-Y. *J. Polym. Sci., Polym. Phys. Ed.* **1988**, *26*, 179.
(20) Jackson, W. J.; Kuhfuss, H. F. *J. Polym. Sci., Polym. Chem. Ed.* **1976**, *14*, 2043.

MA021790V